Observations of Small-Scale Mixing Processes in the Seasonal Thermocline. Part I: Salt Fingering

G. O. MARMORINO

Ocean Dynamics Branch, Acoustics Division, Naval Research Laboratory, Washington, DC 20375

(Manuscript received 7 October 1986, in final form 3 February 1987)

ABSTRACT

Towed conductivity microstructure measurements are examined for evidence of salt fingering in the seasonal thermocline of the Sargasso Sea. Patches of limited-amplitude, narrow-bandwidth signals occur in particular fluid layers about 1 m thick and up to several kilometers in horizontal extent. The finger-like signals occur continuously in the patches but are incoherent between sensors spaced 30 cm apart horizontally. Conductivity gradient spectra rise above background levels in a limited range of wavelengths, peaking at 3 to 5 cm, in a fashion qualitatively similar to Schmitt's spectral model. The density ratio is made favorable for salt fingering within the microstructure patches by finescale variability in the salinity profile. This is consistent with observations by Gargett and Schmitt and also Mack. The vertical convective heat flux estimated from the $(\Delta S)^{4/3}$ laboratory law, where ΔS is the vertical salinity difference across a patch, appears too large when compared with values inferred from either the microstructure measurements themselves or with a flux law based on the vertical gradient across a patch.

1. Introduction

Salt fingering is a small-scale process with large-scale consequences as associated vertical fluxes of heat, salt, and buoyancy can drive intrusions and control water mass characteristics; however, their study in the ocean is still in its infancy and important questions remain about the frequency of their occurrence and how well laboratory results model their behavior. Ocean measurements with towed microstructure sensors have identified salt fingers by their limited amplitude and bandwidth (Magnell, 1976; Gargett and Schmitt, 1982; and Osborn and Lueck, 1985). Gargett and Schmitt found dominant wavelengths and spectral shape in good agreement with Schmitt's (1979) model, and found encouraging support for two laboratory flux laws. Recently, Mack (1985) inferred the existence of salt fingers in the Sargasso Sea (and elsewhere) from repeated vertical profiles with a CTD (Conductivity–Temperature–Depth) instrument. Microstructure was detected presumably because the fingers were tilted from a vertical orientation by vertical shear (see also Gregg, 1980, Fig. 23) or because the CTD descended at an angle to the vertical on account of ship drift. Details of the structure were unresolved, but Mack did find strong support for Schmitt's (1979) contention that finger growth rate is proportional to the density ratio $R_\rho \equiv (\alpha\partial T/\partial z)/(\beta\partial S/\partial z)$, where $\alpha = \rho^{-1}(\partial\rho/\partial T)$ and $\beta = \rho^{-1}(\partial\rho/\partial S)$, by showing that as R_ρ approaches the limiting value of one, the probability of detecting salt-finger-scale temperature fluctuations approaches unity. (See also Schmitt and Georgi, 1982.) Mack points out the need for additional two-dimensional measurements capable of resolving the fingers as well as accurately determining the density ratio.

This paper seeks to provide further insight into the nature of salt-finger microstructure. The measurements were obtained in the seasonal thermocline of the Sargasso Sea with a towed thermistor chain and microstructure conductivity sensors. Sensors were mounted in horizontal pairs, which allowed calculation of coherence and unambiguous separation of real microstructure and spurious signals. Because of the tilting of isopycnals by ubiquitous internal waves, the horizontal tows provide occasional quasi-vertical profiles from which values of R_ρ can be inferred (e.g., Gargett, 1978). The microstructure occurs in thin fluid layers with fingering-favorable values of R_ρ that can be followed for many hundreds of meters horizontally. These long spatial series make possible an accurate determination of the spectral characteristics of the signals. To avoid confusion with the terminology of (convecting) layers and (fingering) interfaces used when discussing double-diffusive staircases, we use the term "patch" to denote the microstructure zones found here.

A companion paper (Marmorino, 1987; hereafter Part 2) examines microstructure from elsewhere in the seasonal thermocline. Those signals have the character of a broadband process (such as turbulence) and occur where the temperature field indicates fluid overturning. Parts 1 and 2 provide a study in contrasts between the processes of salt-fingering and dynamical instability.

2. Instrumentation

Temperature was measured at 75-cm intervals along an inclined tow cable from about 5–90 m depth. At the depths of interest, this gives a vertical separation of about 55 cm between thermistors. One-second averages are used in this work and these have a relative accuracy of about 0.01°C. Towing speed varied from 240 to 295 cm s^{-1}, giving a horizontal resolution for the temperature data of about 2.7 m. The data have been vertically aligned to remove the effect of chain shape. Vertical motion of the chain was negligible over time scales of seconds (the ship-motion band), but could be significant over periods of several minutes (see section 5).

Conductivity data in this study are from an adjacent pair of "dual-needle" probes. Each probe consists of two 1.25-mm diameter forward-facing platinized-platinum electrodes spaced 3 mm apart. The probes have half-power response at a wavenumber between 0.7 and 1 cy cm^{-1} (Okawa and Dugan, 1984) and were sampled at 500 Hz. A probe was positioned at the end of each of two 15-cm-long arms extending horizontally from a streamlined tow body attached to the thermistor chain. When under tow, the two sensors point into the flow, are 30-cm apart in the cross-tow direction, and are behind (but not in the wake of) the chain.

3. Background conditions and selection of data

These data are from a July 1981 cruise in the Sargasso Sea (31°N, 72°W) that includes a crossing of a density front. In the vicinity of the front, microstructure and finestructure signals are relatively intense, occurring jointly in spatially extensive patches (Marmorino et al., 1986; Part 2). North of the front (in this case, the warm side), the patches are much smaller in vertical extent, less energetic, less correlated with each other, and likely more typical of background conditions. It is from these that episodes were chosen for detailed analysis. The sole criterion for selection was that original recordings of (horizontal) conductivity gradient show a persistent signal with relatively constant amplitude. Spurious signals with this characteristic result from biological fouling (Okawa and Dugan, 1984) but were avoided by examining adjacent probes. All results shown here are from two probes—A and B—located below thermistor number 125, at a depth of about 60 m. Additional results can be found in Marmorino (1986, unpublished manuscript).

CTD stations were occupied before and after towing operations. Figure 1 shows the CTD cast made closest in time and space to the microstructure measurements. The T–S diagram (not shown) is consistent with those found by Wahl and Teague (1985) for August–October in the area of 30°–32°N, 71°–74°W, suggesting that the conditions portrayed are fairly typical of the Sargasso Sea. As shown in Fig. 1, salt fingering is impossible above the salinity maximum at 70 m except in association with unresolved salinity intrusions (thickness < 5 m). Below the salinity maximum, salt fingering is possible but likely poorly developed as the large-scale value of R_ρ is about 10 (e.g., Gargett and Schmitt found salt fingering signatures where $R_\rho \sim 3$ but not where it was 8).

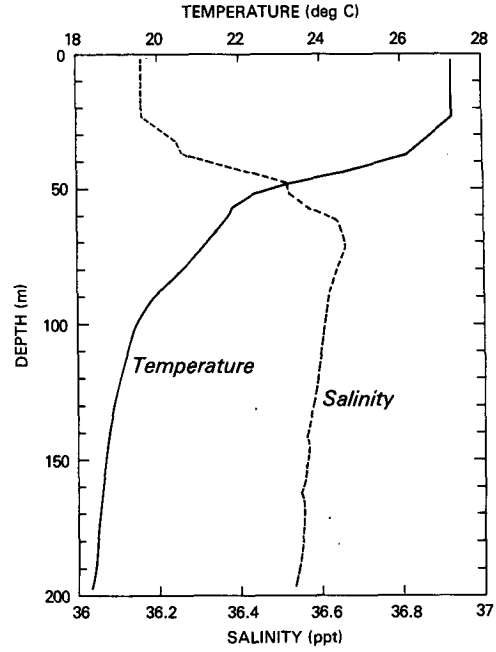

FIG. 1. Temperature and salinity profiles (modified from Trump et al., 1985) made 3 days after the towing operations and about 30 km east of the microstructure measurements. Below the salinity maximum (70 m), conditions are favorable for salt fingering but values of density ratio are large. The microstructure observations are from depths shallower than 70 m. There salt fingering occurs as a result of finescale variability in the salinity profile, unresolved in the 5-m averaged data shown.

Acoustic Doppler current measurements show that, for the periods of interest, the velocity at 60 m depth is 48 cm s^{-1} at 208 ± 2 deg. The vertical shear varies from about 0.004 to 0.008 s^{-1} over scales of 10 m or more, likely the result of inertial waves. For a vertical temperature gradient of 0.001°C cm^{-1}, this gives a 7-m Richardson number of between 5 and 20.

4. Analysis methods and errors

This section discusses errors involved in computing salinity from the data and inferring the density ratio from changes in temperature and salinity along the tow path. The density ratio is a fundamental indicator of the nature and strength of double-diffusive activity. Care has been taken in its calculation to alleviate shortcomings in the data. On the whole, the results have reasonable magnitudes and show realistic spatial

variability; still, they must be treated with some caution.

Spikes in the conductivity data result from random encounters with particulate matter (e.g., Fig. 2). These were removed with a de-spiking scheme (Marmorino et al., 1986) before 1-s averages were calculated. The redundant conductivity measurement was then used to reduce the relative error in conductivity to about 0.003 mS cm^{-1}. Differences in conductivity are taken as significant only when they exceed this value.

The conductivity sensors were configured with an unknown vertical offset relative to the thermistors. It was necessary to take this into account so that the part of the conductivity change induced by temperature alone could be removed and salinity determined from what remained. The offset was estimated by maximizing the correlation between an interpolated temperature and the observed conductivity. This typically produced offsets of 20 to 30 cm and a correlation coefficient greater than 0.99. This corrective measure will not work if the temperature profile contains finestructure on scales comparable to the thermistor spacing. In that case, spurious salinity variations will be induced by features in the conductivity records that are inadequately compensated for by the linearly interpolated temperatures. If small-scale variability is intermittent, salinity errors will be localized, allowing real salinity variations along the tow path to be extracted from the data.

Following Ruddick (1983), we define the Turner angle, Tu, as the four-quadrant arctangent of $(N_T^2 - N_S^2)/(N_T^2 + N_S^2)$. The Turner angle and density ratio are then related by $R_\rho = -\tan(\mathrm{Tu} + 45°)$. In our work, $N_T^2 = \pm g\alpha\Delta T/\Delta x$ and $N_S^2 = \pm g\beta\Delta S/\Delta x$. The observed local $\partial T/\partial z$ determines the sense of the T stratification. The sense of the S stratification is then inferred from the relative signs of ΔT and ΔS. Constant values of $\alpha = 2.85 \times 10^{-4}$ $(°C)^{-1}$ and $\beta = 7.4 \times 10^{-4}$ ppt^{-1} were used. The horizontal scale Δx must be sufficiently long to yield significant horizontal differences (see below), yet short enough to provide as local a value as possible. The results shown use $\Delta x = 35$ m, but experimentation with longer values gave confidence in the general trends in the results.

The Turner angle was calculated only if horizontal changes exceeded the expected errors: $\Delta T > 1.2 \times 10^{-3}$ °C; $\Delta S > 2.0 \times 10^{-3}$ ppt; $\Delta\rho > 5.0 \times 10^{-6}$ gm cm^{-3}; and $T_z > 2.0 \times 10^{-4}$ °C cm^{-1}. A further constraint on ΔS was that the values from both probes agree in sign and to within 30% in magnitude. In order to show the sensitivity of the results to our treatment of the vertical offset, presented values of Tu use three different offsets: the value that maximizes the temperature–conductivity correlation, a value 10 cm less, and a value 10 cm more. Some local values of Tu do appear spurious (e.g., values in the overturning regime or stable values amidst microstructure). It is not clear whether these occur because the horizontal gradient is accurately determined but is an inappropriate representation of the local vertical gradient (the case if the T–S relationship changes horizontally) or because of other errors.

5. Observations

Eight microstructure patches have been examined in detail. The examples shown are representative of the measured extents of the patches, the background finescale stratification, and the spectral characteristics of the signals.

a. Two-dimensional view

Figure 2 shows a 1.5-m thick patch lying in the temperature range $24.80° < T < 24.94$°C. (The patch boundaries are defined by identifying the isotherms that are crossed when the signals appear or disappear.) The patch is transected first at the beginning of the figure, then again 200 m farther along. Microstructure within nearly the same temperature range is observed prior to the Fig. 2 period (over a 200 m extent) and about 1 km beyond the end of that period, as shown in Fig. 3. Shading is used to suggest that microstructure occurs within this temperature range throughout the period of the two figures. Also in Fig. 2 is a thinner patch ($25.02° < T < 25.06$°C) at least 100 m long. How much farther it extends is not known, so it is shown shaded for only a short distance. Its temperature range is sampled about 1.5 km later in the tow and no microstructure is found, but microstructure does occur between 25.06° and 25.14°C.

Warmer water is sampled over the periods shown in Figs. 2 and 3 as the chain gradually shoals by about 1 m. Overall, salinity decreases slightly along the tow (clearest in Fig. 2), implying a salinity decrease with height and conditions unfavorable for salt fingering. This agrees with CTD information. However, salinity does increase with height over short intervals as the result of salinity maxima near the upper edges of the patches. These finescale vertical variations of salinity give values of R_ρ in the finger regime (Turner angles between 45 and 90 deg) when microstructure signals are observed, and values in the stable regime ($-45 < \mathrm{Tu} < 45$ deg) otherwise.

b. Microstructure characteristics

The microstructure signals from the conductivity sensor pair are very similar (see later spectra) and change only slowly along the tow. This implies the generating mechanism acts fairly uniformly through the patch. There is, for instance, no evidence for the break-up of the signals into smaller bands (Linden, 1978). The signal amplitude gradually increases and decreases as the probes enter and leave a patch. This slowly varying behavior can also be seen in Gargett

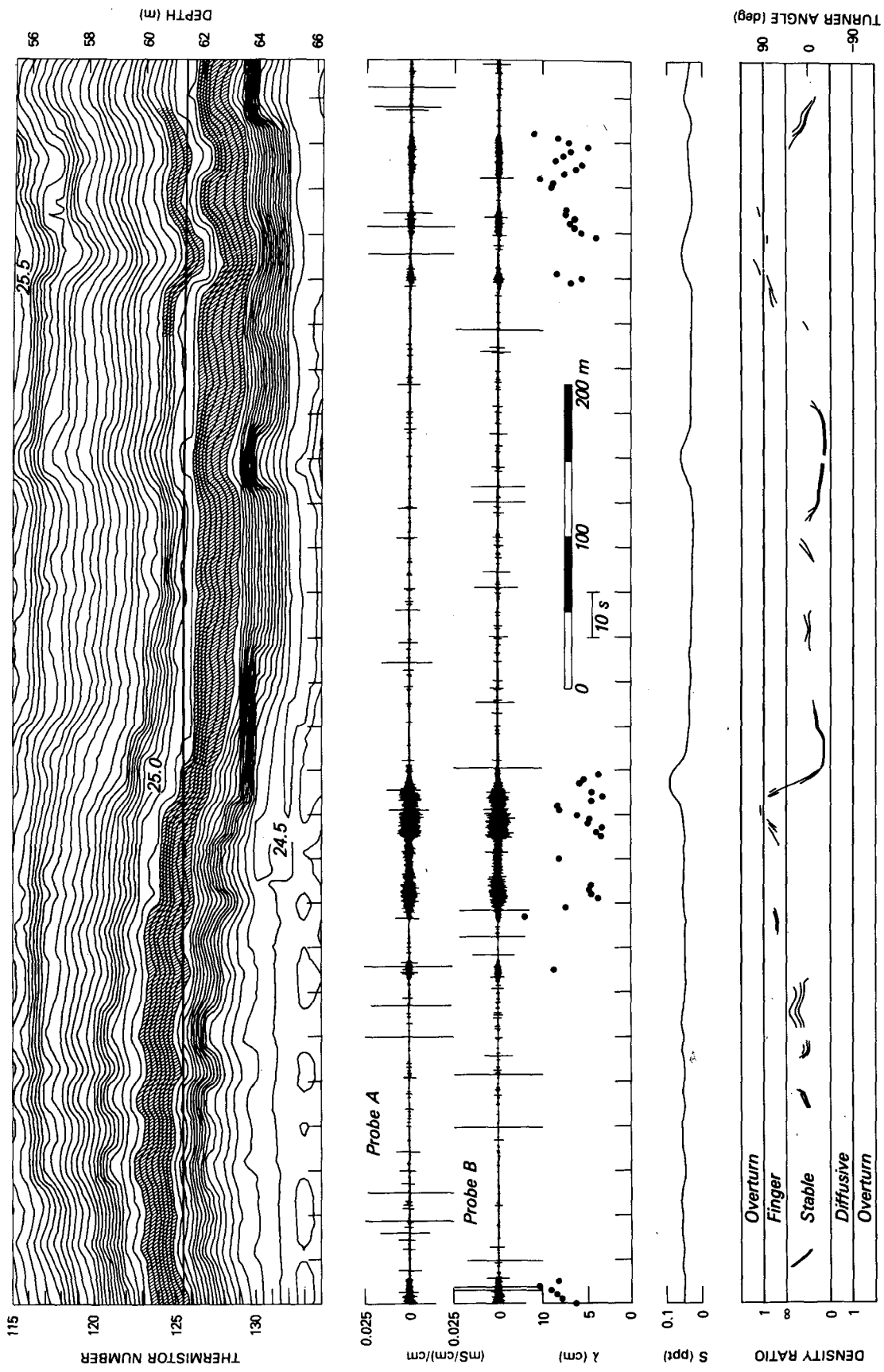

FIG. 2. The path (heavy line) of a conductivity sensor pair through a temperature section (upper panel) along with the conductivity gradient signals (lower panels), their dominant wavelength, the relative salinity, and the inferred density ratio. Temperature is contoured at 0.02°C intervals. The amplitude- and frequency-limited signals of conductivity gradient are identified as salt fingers. They appear bounded by the 24.80° and 24.94°C and by the 25.02° and 25.06°C isotherms. These fluid layers are shaded for reference. The wavelength (λ) of the signals is shown only when the variability among successive data segments is small. Two relative salinity series are drawn but, at this scale, they are indistinguishable from one another. See text for details.

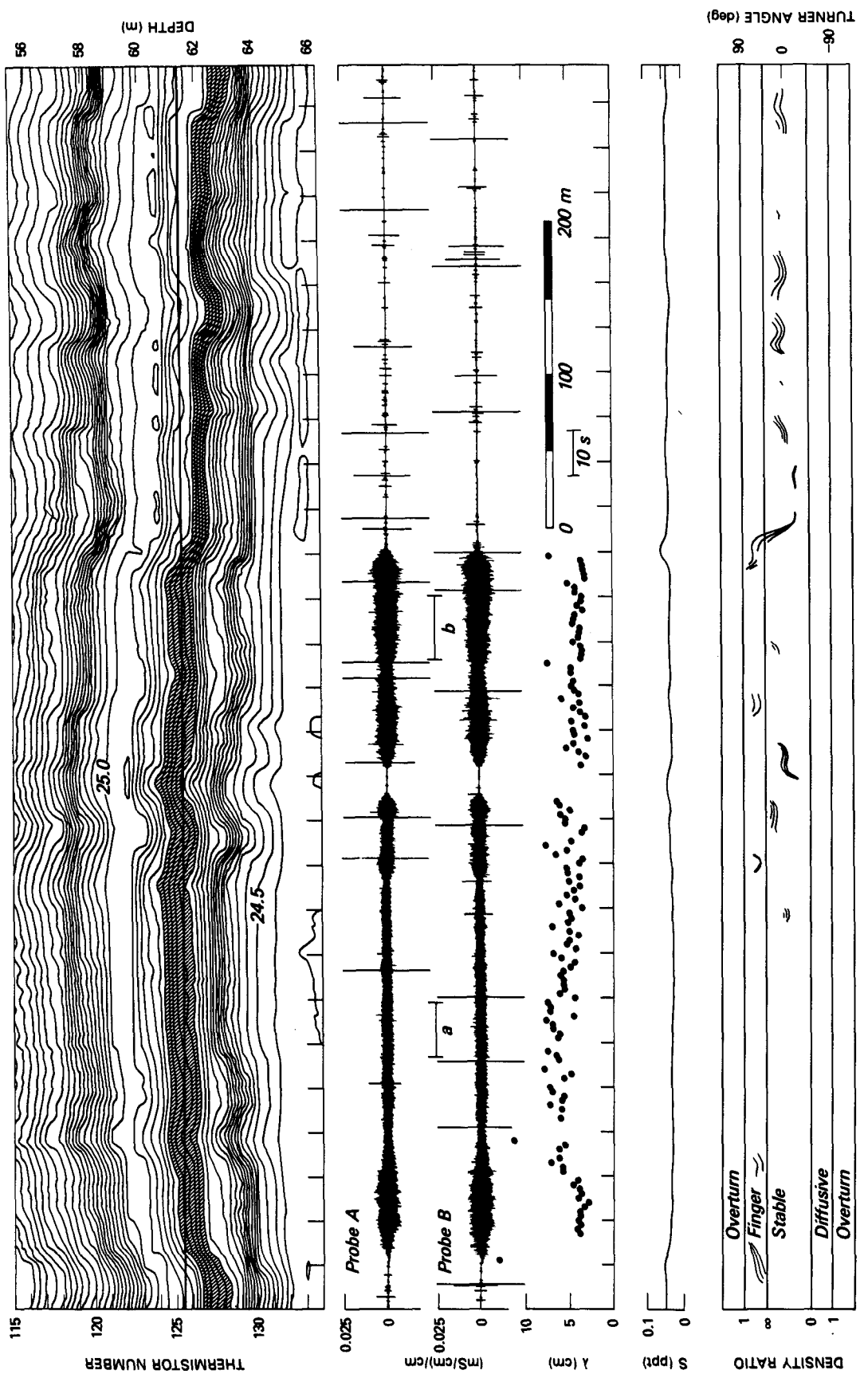

FIG. 3. As in Fig. 2, but beginning about 370 m beyond the end of Fig. 2. The shaded microstructure patch is bounded by the 24.80° and 24.88°C isotherms, about the same as the lower patch in Fig. 2.

and Schmitt's Fig. 3a and Osborn and Lueck's Fig. 17, and contrasts with the abrupt change in amplitude expected across the boundary between turbulent and laminar fluid. (Compare, for example, the "salt finger" and "turbulent" parts of Gargett and Schmitt's figure.)

Near edges of a patch the signals often become asymmetric. A good example is shown in Fig. 4. The inset offers a possible explanation. It shows a vertical cross section through a hypothetical field of salt fingers, qualitatively similar to one of Piacsek and Toomre's (1980) numerical simulations during exponential growth phase. The point of the sketch is that not all buoyant fingers rise to the same height, nor do all heavy fingers sink to the same depth. Hence, a transect along depth z_3 would show intermittent cold, relatively fresh spikes corresponding to encounters with ascending fingers. Qualitatively, this agrees with the observations from the upper edge of the patch (the bracketed section at the right in the figure). The fluctuations are observed to be more symmetrical near the middle of the patch, corresponding to a transect along depth z_2. They become asymmetrical again near the lower part of the patch (depth z_1). A referee suggested that the changes in the signals might be evidence for convective plumes. As there are no well-mixed (convecting?) layers adjacent to the patches, this is a difficult distinction to make.

Close examination of the conductivity signal pairs revealed no clear visual correlation, and cross-spectra on a number of data segments gave no significant coherence. Linden (1974) found in the laboratory that, for a steady shear flow, salt fingers were aligned into vertical sheets oriented parallel to the shear. In our case, the angle between the shear (presumably low-frequency) and the sample path varied from nearly 0 to 60 deg. No coherence being found suggests that sheets did not exist in any regular pattern over distances comparable to the 30-cm sensor spacing.

The dissipation rate $\chi = 2\kappa\langle(\nabla T)^2\rangle$ can be estimated from the conductivity gradient signals, c_x. The fingers are assumed to be horizontally isotropic and vertically oriented; therefore, $\langle(T_x)^2\rangle = \langle(T_y)^2\rangle = \langle(c_x)^2\rangle$ and $\langle(T_z)^2\rangle = 0$. For the microstructure in Figs. 2 and 3, values of χ vary from (0.4 to 6) $\times 10^{-8}$ $(°C)^2$ s^{-1}. The temperature fluctuations are less than about 5 m °C or about 0.05 times the temperature contrast across the patch. We define the Cox number as $C = 2\langle(T_x)^2\rangle/(\langle T_z\rangle)^2$. As $T_z \sim 10^{-3}$ °C cm^{-1}, values of C vary from about 2 to 20.

c. *Spectral shape and dominant wavelength*

Most of the observed microstructure spectra are quite similar. Examples are shown (Fig. 5) for the periods

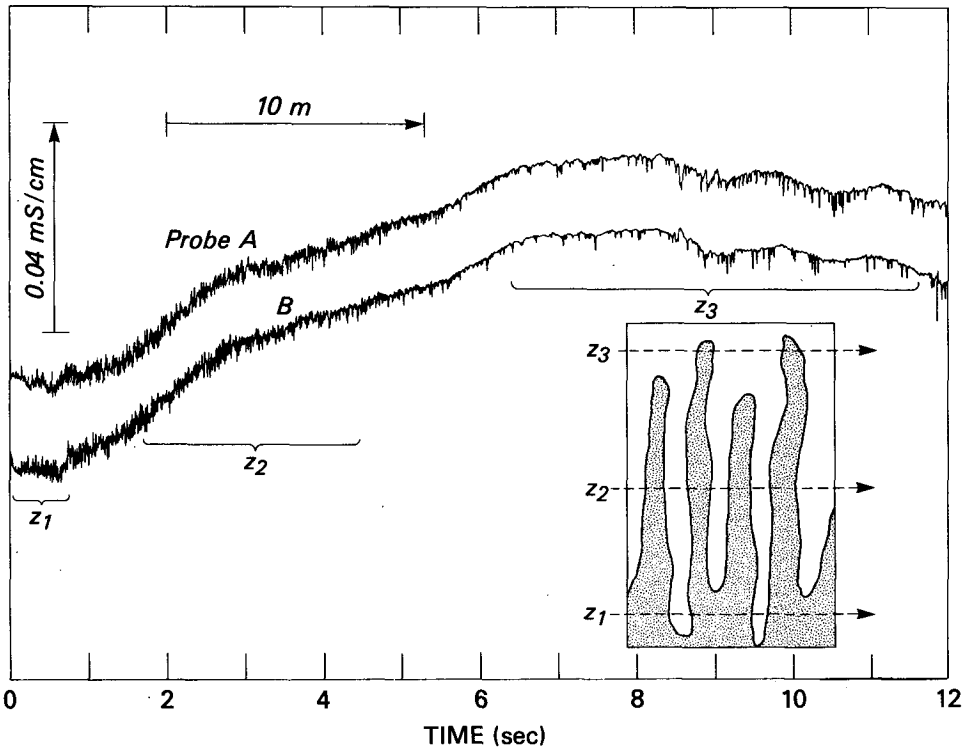

FIG. 4. Time series of conductivity measured as the probes moved upwards through a microstructure patch. Notice the cold spikes in the right half of each series where the probes are in the warmest water. Sampling a hypothetical field of salt fingers (inset) at the depths (z_i) shown would yield time series similar to those observed. The shaded part in the inset represents relatively cold, fresh water.

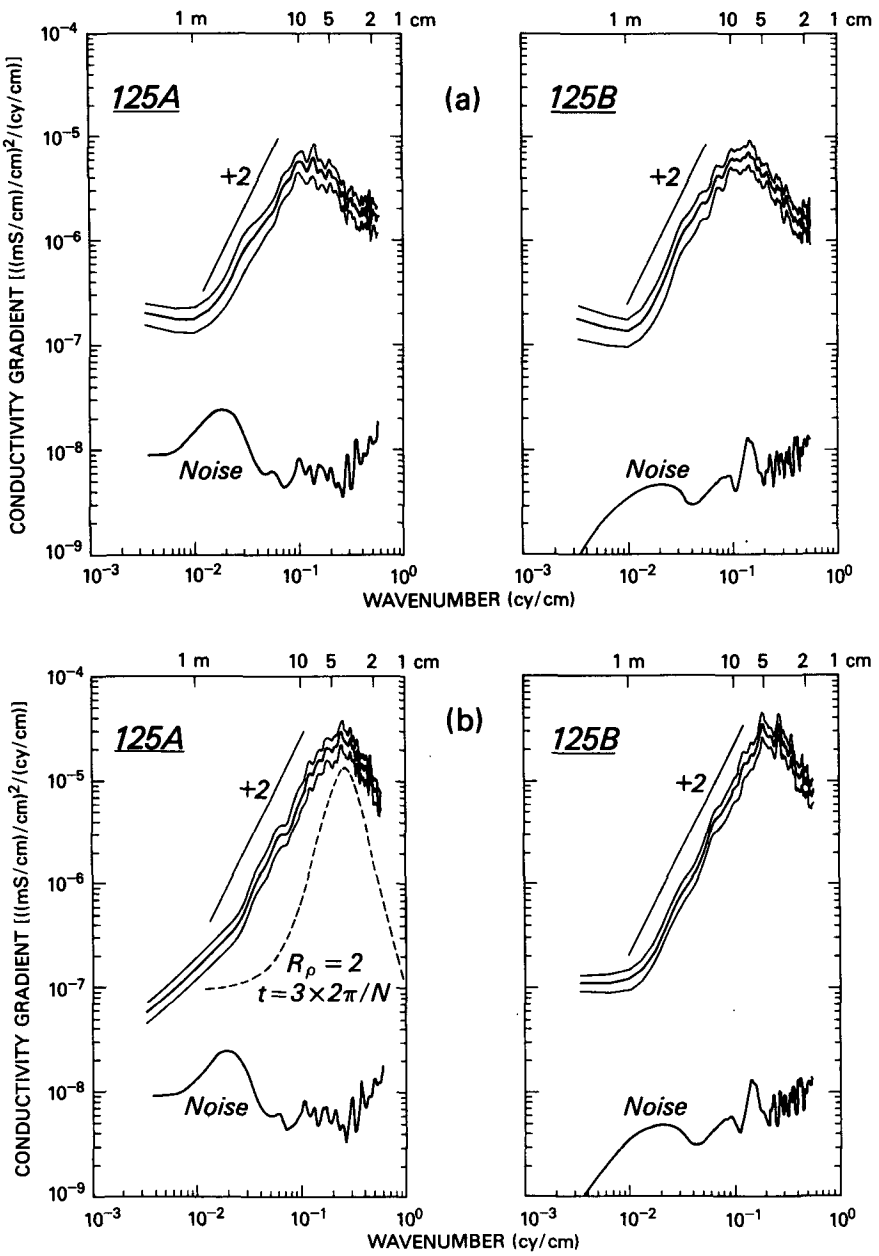

FIG. 5. Microstructure spectra for periods "a" and "b" in Fig. 3 shown side by side for both probes. Solid curves show the ensemble mean with standard error bounds. For reference the dashed curve shows a temperature gradient spectrum modeled according to Schmitt (1979) with a seed level of 10^{-7} (°C cm^{-1})^2/(cy cm^{-1}), a density ratio of 2, and a growth period of 3 buoyancy periods.

marked "a" and "b" in Fig. 3. Those periods were chosen to be free of obvious "particulate" spikes for both probes; the results do not change significantly for longer series. "Noise" levels were calculated over nearby quiet periods. The spectra from the two probes are identical to within the standard error bounds shown, except at low-wavenumber where the effect of noise is a concern. The spectra increase as (wavenumber)$^{+2}$, reaching a peak at a wavelength of about 4 cm (period b) to 7 cm (period a). A turbulent spectrum would increase as (wavenumber)$^{+1}$. These spectra are similar to those of Gargett and Schmitt, but different from Osborn and Lueck's (their Fig. 16) which has a less steep slope.

For comparison, temperature spectra were "grown" using Schmitt's (1979) model. The example in Fig. 5b uses an initial "seed" level of 10^{-7} (°C cm^{-1})^2/(cy cm^{-1}), comparable to the lowest levels in the observed

spectra, and a value of $T_z = 0.001°C\ cm^{-1}$. As there is no evidence for a particular orientation of finger sheets, the modeled finger wavenumbers are given by Schmitt's Eq. (13). For R_ρ values in the range observed, the modeled spectra are narrow band and have peaks at wavelengths of 3–4 cm. Those are smaller than the observed values in Fig. 5 but close to the mode for the dataset (see below). The model results match maximum observed spectral levels if allowed to evolve for 3 to 5 buoyancy periods, consistent with what Gargett and Schmitt found. A measure of the peakedness of a spectrum is the quantity Q, defined as peak wavenumber divided by the half-power bandwidth. The model spectra have Q values of about 1.5, larger than observed values of about 1. Likewise, the model slope prior to the peak is steeper than observed. This suggests that a wider range of finger sizes are observed in the ocean data, possibly because the fingers are more randomly oriented than the model allows.

To systematically explore the variation in dominant wavelength, spectra were computed over short (35-cm long) data segments from both probes. Wavenumbers corresponding to spectral peaks were tabulated and averaged each second. We were careful to eliminate contaminated data, poorly defined peaks, and data too close to noise levels; furthermore, we required half the number of segments per second to have peaks. Sample results are shown in Figs. 2 and 3. A histogram (not shown) of peak wavelengths for all the patches studied (about 2.3 km of data) has a mode of 3.5–4.0 cm with nearly half the peaks occurring between 3 and 5 cm. Although the smallest resolved wavelength is only about 1.6 cm, the relative sparsity of values less than 3 cm seems to be real since the variability amongst individual spectra was low. Variations in the peak wavelength tend to be reflected in the microstructure gradient (e.g., Fig. 3). This can be accounted for by assuming conductivity varies as $\sin(kx)$, in which case the gradient is proportional to wavenumber, k. Why this variability in wavelength (or gradient) exists is not clear from the data.

d. Vertical buoyancy flux due to temperature

Because of the potentially significant role salt fingering may play in redistributing heat and mass, it is important to validate the proposed formulations for vertical flux. Gargett and Schmitt (1982) give three ways of computing the buoyancy flux due to temperature, αF_T. In our notation, these are,

$$(\alpha F_T)_1 = \alpha\kappa\langle(\nabla T')^2\rangle/T_z \quad (1)$$

$$(\alpha F_T)_2 = \alpha\nu A R_f T_z \quad (2)$$

$$(\alpha F_T)_3 = a(g\kappa)^{1/3} R_f(\beta\Delta S)^{4/3} \quad (3)$$

Here $F_T = \langle w'T'\rangle$ is the *convective* heat flux, where w' and T' are fluctuations in vertical velocity and temperature. We will assume temperature and conductivity fluctuations are identical; κ is the thermal diffusivity, ν is the kinematic viscosity, g is the gravitational acceleration, T_z is the average vertical temperature gradient through the patch, and ΔS is the salinity difference across it. We use Gargett and Schmitt's values for the flux ratio, R_f, the "constant" a (their C), and Stern's (1969) collective-instability parameter A. These values are 0.68, 0.07, and 1.2, respectively. Equation (1) is based upon the temperature gradient variance of the microstructure itself and may underestimate the flux by about a factor of two. Both (2) and (3) have been verified in the laboratory (Gargett and Schmitt, 1982).

For the measurements in Fig. 3, typical values are $\langle(\nabla T')^2\rangle = 4 \times 10^{-6}\ (°C/cm)^2$ and $T_z = 10^{-3}\ °C\ cm^{-1}$. This gives $(\alpha F_T)_1 \sim 2 \times 10^{-9}\ cm\ s^{-1}$. For comparison, Gargett and Schmitt calculate $(2–7) \times 10^{-9}\ cm\ s^{-1}$ for their data. Now the ratio of (1) to (2) is $\kappa C/\nu A R_f \sim C/6$; so the two flux estimates are equivalent for $C = 6$, or $C = 3$ if (1) underestimates the flux. As a typical Cox number is about 4, the two flux estimates are approximately the same for these data. This is similar to Gargett and Schmitt's result.

In method 3, we use $\Delta S = 0.05$ ppt on the basis of the maximum observed salinity changes. This value is likely correct to within a factor of two. Equation (3) then gives $(\alpha F_T)_3 \sim (0.053)(\beta\Delta S)^{4/3} \sim 6.5 \times 10^{-8}\ cm\ s^{-1}$, about 30 times the estimates from (1) or (2). We conclude that the laboratory-based four-thirds power law gives a flux *significantly larger* than the ocean data support. This discrepancy may be related to the fact that the salt finger patches are much thicker than the interfaces studied in the laboratory. It should be noted that Gargett and Schmitt had some difficulty in reconciling results based on a ΔS value determined over their entire fingering patch with their other calculations.

6. Summary

This paper has presented an examination of elongated patches of microstructure occurring in relatively quiescent sections of the seasonal thermocline of the Sargasso Sea. The evidence summarized below suggests the microstructure signals are salt fingers. The inferred 1-m vertical scale of the patches appears to be set by finescale interleaving in the salinity profile, consistent with results of Gargett and Schmitt (1982) and Mack (1985). The total horizontal extent of the layers was unmeasured, but one layer was repeatedly sampled over several kilometers. For comparison, Gargett and Schmitt observed a salt finger patch at least 300 m long. Similar to Gargett and Schmitt, the vertical convective heat flux inferred from the microstructure measurements is comparable to a laboratory flux estimate based on the vertical temperature *gradient* across the patch; however, another laboratory law based upon the vertical salinity *difference* across the patch gives too large a flux.

The characteristics of the measurements that support interpreting the microstructure as salt fingers are

(i) The signals are confined to particular fluid layers. Ocean turbulence is distributed randomly with respect to the finescale stratification (e.g., Gregg, 1980).

(ii) The signals are observed continuously in the patch, changing only gradually in the horizontal and vertical, and exhibit no significant amplitude change between probes spaced 30-cm apart in the cross-tow direction. Turbulence tends to be much more spatially intermittent, even within a single patch.

(iii) The character of the signals near the patch edges suggests a convective process (such as salt fingering).

(iv) The signals occur where the density ratio is favorable for salt fingering; no signals are observed in neighboring fluid layers which are stable to double diffusion.

(v) The two-dimensional temperature field shows no evidence of finescale stirring, e.g., there are no inversions or closed contours and no overturning internal waves; nor is the Richardson number (based on 7-m vertical shear), low enough to favor flow instabilities.

(vi) The Cox number in the patches is about 10, which is too low to support turbulence (Gibson, 1982).

(vii) The observed spectra are qualitatively similar to Schmitt's (1979) salt finger model which produces narrow-band spectra with peaks at wavelengths of 3 to 5 cm. Turbulence spectra do not have as steep a slope as is observed.

No attempt has been made to examine the dataset systematically to uncover all potential occurrences of salt fingering, nor has the source of finescale interleaving been addressed. Marmorino et al. (1986) suggest that turbulent processes make the dominant contribution to total observed levels of microstructure variance and Cox number, but this ignores the difficult questions of which process has the greater frequency of occurrence and which produces the greater net vertical mixing. The selected analyses presented here, and for the case of turbulent mixing in Part 2, are first steps toward answers.

Acknowledgments. This is a contribution to the Naval Research Laboratory's Finescale Variability Program. The quality of the conductivity and temperature data is a result of the engineering skill of B. Okawa, W. Morris, and others associated with the Ocean Dynamics Branch. One particular referee was exceptionally helpful in improving the clarity of the manuscript. Typing was done by C. Pasquini.

REFERENCES

Gargett, A. E., 1978: Microstructure in an upper ocean frontal region. *J. Geophys. Res.*, **83,** 5123–5133.

——, and R. W. Schmitt, 1982: Observations of salt fingers in the central waters of the Eastern North Pacific. *J. Geophys. Res.*, **87,** 8017–8029.

Gibson, C. H., 1982: On the scaling of vertical temperature gradient spectra. *J. Geophys. Res.*, **87,** 8031–8038.

Gregg, M. C., 1980: Microstructure patches in the thermocline. *J. Phys. Oceanogr.*, **10,** 915–943.

Linden, P. F., 1974: Salt fingers in a steady shear flow. *Geophys. Fluid Dyn.*, **6,** 1–27.

——, 1978: The formation of banded salt finger structure. *J. Geophys. Res.*, **83,** 2902–2912.

Mack, S. A., 1985: Two-dimensional measurements of ocean microstructure. *J. Phys. Oceanogr.*, **15,** 1581–1604.

Magnell, B., 1976: Salt fingers observed in the Mediterranean outflow region (34°N, 11°W) using a towed sensor. *J. Phys. Oceanogr.*, **6,** 511–523.

Marmorino, G. O., 1987: Observations of small-scale mixing processes in the seasonal thermocline. Part II: Wave breaking. *J. Phys. Oceanogr.*, **17,** 1348–1355.

——, J. P. Dugan and T. E. Evans, 1986: Horizontal variability of microstructure in the vicinity of a Sargasso Sea front. *J. Phys. Oceanogr.*, **16,** 967–980.

Okawa, B. S., and J. P. Dugan, 1984: Contamination of conductivity measurements by waterborne particles. *Ocean Eng.*, **11,** 265–279.

Osborn, T. R., and R. G. Lueck, 1985: Turbulence measurements with a submarine. *J. Phys. Oceanogr.*, **15,** 1502–1520.

Piacsek, S. A., and J. Toomre, 1980: Nonlinear evolution and structure of salt fingers. *Marine Turbulence,* J. C. J. Nihoul, Ed., Elsevier, 378 pp.

Ruddick, B., 1983: A practical indicator of the stability of the water column to double-diffusive activity. *Deep-Sea Res.*, **30,** 1105–1107.

Schmitt, R. W., 1979: The growth rate of super-critical salt fingers. *Deep-Sea Res.*, **26A,** 23–40.

——, and D. T. Georgi, 1982: Finestructure and microstructure in the North Atlantic Current. *J. Mar. Res.*, **40,** 659–705.

Stern, M. E., 1969: Collective instability of salt fingers. *J. Fluid Mech.*, **35,** 209–218.

Trump, C. L., B. S. Okawa and R. H. Hill, 1985: The characterization of a mid-ocean front with a Doppler shear profiler and a thermistor chain. *J. Atmos. Oceanic Technol.*, **2,** 508–516.

Wahl, R. J., and W. J. Teague, 1983: Estimation of Brunt–Väisälä frequency from temperature profiles. *J. Phys. Oceanogr.*, **13,** 2236–2240.